Spatiotemporal Filter Velocimetry with Arbitrary-Shaped Measurement Region for Accurate Measurement in the Vicinity of a Boundary

S. Hosokawa[1,*]

1: Dept. of Sociatal Safety Science, Kansai University, Japan
* Correspondent author: hosokawa@kansai-u.ac.jp

Keywords: Deformed drop, Surfactant, Spatiotemporal filter velocimetry

ABSTRACT

Viscous stress at a boundary or an interface is a source of drag acting on a body or a fluid particle and therefore its measurement is of great importance for understanding the motion of the body or the fluid particle. In this study, spatiotemporal filter velocimetry (SFV) is extended to arbitrary quadrilateral measurement areas fitted to an interface shape for accurate measurement of flow about a deformed drop, and it is applied to flows about single drops of glycerol-water solution falling in stagnant silicon oil under clean and contaminated conditions. As a result, we confirmed that SFV enables us to measure velocity distribution about a single deformed drop, and it has the potential to evaluate viscous stress at a boundary or an interface in complex structures. The measured results show that the flow inside the drop and the interfacial velocity become weak as the bulk concentration of surfactant increases. However, the internal circulation in an ellipsoidal drop remains even at the high surfactant concentration condition under which the internal circulation in a spherical drop is fully damped.

1. Introduction

Viscous stress at a boundary or an interface is a source of drag acting on a body or a fluid particle. Although direct measurement of local viscous stress at the surface of moving body is not easy task, the stress could be evaluated from the velocity distribution in the vicinity of the surface, i.e., the velocity gradient at the surface. PIV is widely used for measuring velocity distribution. However, the accuracy of the evaluated velocity gradient tends to decrease when the surface shape becomes complex. This is mainly due to the rectangular measurement region in regular grid. Hosokawa and Tomiyama (2012) developed Spatiotemporal filter velocimetry (SFV) for accurate velocimetry, and applied to flow about single spherical drops (Hosokawa et al., 2017). They succeeded in accurate viscous stress evaluation based on the measured velocity distribution by using boundary-fitted measurement regions in a cylindrical coordinate. Hosokawa et al. (2018) demonstrated accurate evaluation of drag force acting on a spherical drop by coupling SFV with a pressure

evaluation method based on velocity distribution. Although SFV have a potential for accurate evaluation of viscous stress at a boundary or an interface, it has been demonstrated only for simple interfaces such as a plane or a sphere.

In this study, SFV is extended to arbitrary quadrilateral measurement region fitted to an interface shape and applied to deformed single drop falling in stagnant liquid to demonstrate accurate velocity measurement in the vicinity of deformed interface.

2. Experimental Method

Figure 1 shows the principle of SFV, which processes time-series particle images recorded by a high-speed camera. A spatiotemporal filter $F_{SF}(x,y,t)$, which is a cyclic function in space, is multiplied to an intensity distribution $I(x,y,t)$ of an image in an interrogation area, and the resultant intensity distribution is integrated in the interrogation area to obtain the integral intensity $I_{SF}(x_c, y_c, t)$ (spatiotemporal filtering step):

$$I_{SF}(x_c, y_c, t) = \int_{y_c-\frac{\Delta y}{2}}^{y_c+\frac{\Delta y}{2}} \int_{x_c-\frac{\Delta x}{2}}^{x_c+\frac{\Delta x}{2}} I(x, y, t) F_{SF}(x, y, t) dx dy \qquad (1)$$

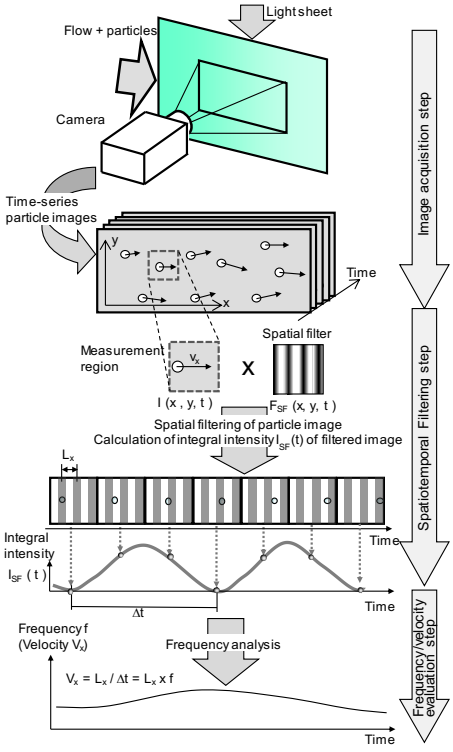

Figure. 1 Principle of spatiotemporal filter velocimetry.

where t is the time, (x_c, y_c) the center position of the interrogation area, and Δx and Δy are the sizes of the area in x and y directions, respectively. When $F_{SF}(x, y, t)$ is a periodic function (period L_x) with respect to x (e.g. $\cos(2\pi x/L_x)$) and a particle with velocity v_x moves in the area, $I_{SF}(x_c, y_c, t)$ periodically fluctuates with the frequency v_x/L_x. Hence, the frequency estimation of I_{SF} yields particle velocity (frequency/velocity evaluation step). The perpendicular velocity component v_y can be measured by using a cyclic function with respect to y as F_{SF}. Thus, we can evaluate two velocity components of each particle in an arbitrary interrogation area in the imaging plane from the time-series particle images. The direction of velocity can be determined by using a moving filter function like the frequency shift in LDV measurements. In this study, we use a cosine function for F_{SF}, and a wavelet analysis is adopted to evaluate the frequency of I_{SF}. Details of SFV can be found in Hosokawa and Tomiyama (2012) and Hosokawa et al. (2017).

In SFV measurements of flow containing deformed interfaces or curved walls, the presence of an interface or a wall surface in an interrogation area is apt to cause measurement errors. Hence, the measurement accuracy and resolution in the vicinity of an interface or surface tend to be lower than those away from the interface/boundary in spite of the importance of the flow near the interface/wall. SFV is, therefore, extended to a general curvilinear coordinate as shown in **Figure 2**. Interrogation areas are formed to fit the interface/boundary, and therefore, the areas are not rectangles but arbitrary shapes. The spatiotemporal filter F_{SF} in the curvilinear coordinate (ξ, η), is projected onto the non-rectangular interrogation area to obtain I_{SF}:

$$I_{SF}(x_c, y_c, t) = \iint I(x, y, t) M(x, y, t) F_{SF}(\xi(x, y, t), \eta(x, y, t), t) dx dy \qquad (2)$$

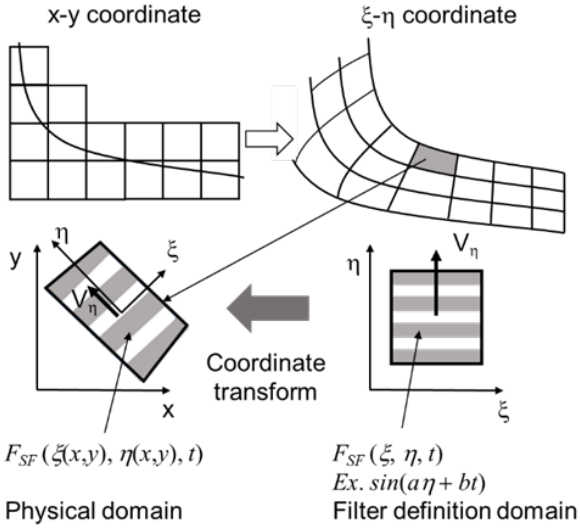

Figure. 2 SFV for boundary fitted interrogation area.

where M is the window function which takes 1 and 0 in the inside and the outside of the interrogation area, respectively. The area of the integration is an arbitrary region which contains the interrogation area. The velocity in the (ξ, η) plane can be evaluated from the frequency of fluctuating I_{SF}. In the programming of the SFV processing, the arbitrary-shaped interrogation area was approximated by the quadrilateral with the same nodal points, and the homography transformation was used for the transformation of F_{SF}. The velocity is calculated from the frequency and the homography matrix.

SFV was applied to flows about single drops of glycerol-water solution (53.5 wt%, viscosity: μ_D = 6.13 mPa s, density: ρ_D = 1132 kg/m^3) falling in stagnant silicone oil (Shinetsu Silicone, KF-96-300cs; viscosity: μ_C = 299 mPa s, density: ρ_C = 967 kg/m^3) in a rectangular container (170(W) x 170(D) x 500(H) mm). **Figure 3** shows the schematic of the experimental apparatus. Millipore water was used to prepare the glycerol-water solution. The concentration of the glycerol-water solution was determined so as to match the refractive index of the solution with that of the silicone oil (Ninomiya and Yasuda, 2006). Silicon dioxide particles (mean diameter: 3 μm) were added to both fluids as tracer particles. Rhodamine B was dissolved in the glycerol-water solution at the concentration of 5.0x10^{-3} mol/m^3 to distinguish the drop region from the other in visualized images. The drop was released from the nozzle located at the center of the cross-section of the container just below the surface of the silicone oil. The drop diameter was 8, 17, and 27 mm for spherical and ellipsoidal drops, respectively. The temperatures of the fluids were fixed at 25 $\pm$ 0.5 ^{o}C.

The vertical center plane of the drop was visualized by a laser sheet (thickness: 0.2 mm, width: 25 mm, wavelength: 532 nm) irradiated from the bottom of the container. The particle images were recorded by a high-speed camera (Photron, FASTCAM SA-X2, frame rate: 12500 fps, resolution: 0.02 mm/pixel), and the velocity distributions were measured by SFV. The velocity measurements were carried out at y = 250 + 10 mm below the nozzle tip. The drop reached a terminal condition before it reached y = 150 mm. The second camera located perpendicular to the high-speed camera was used to check whether the laser sheet passed through the center plane of the drop. The size of the interrogation region was about 0.4 mm in the normal direction and about 0.7 mm in the tangential direction. Velocity in the regions far from the interface was measured by using a rectangular area (0.4 x 0.4 mm). The uncertainty in SFV measurement was confirmed to be less than 5 % in our previous study (Hosokawa and Tomiyama, 2012).

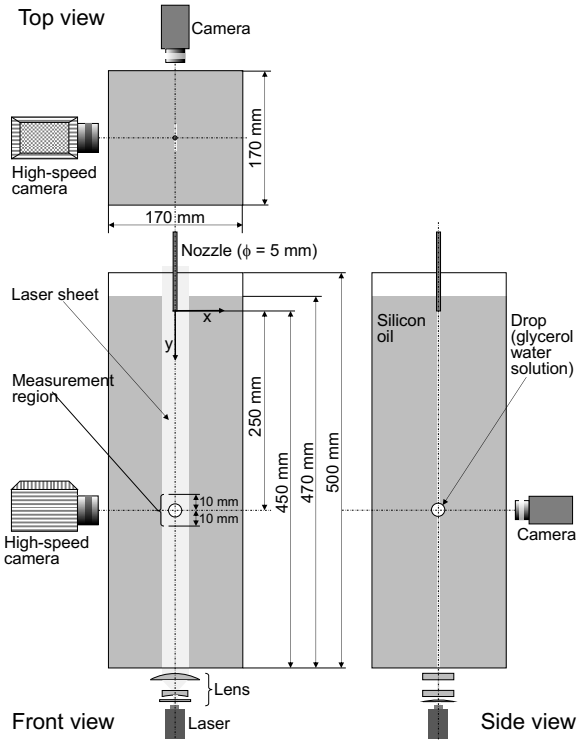

Figure. 3 Experimental setup.

3. Results and Discussion

Figure 4 shows the measured velocity distributions by using a cylindrical coordinate and arbitrary quadrilateral measurement areas in the vicinity of the interfaces. **Figure 5** shows the interfacial velocities $V_{\theta int}$, the velocity gradients dV_θ/dr, and the Marangoni stress $\Delta\tau_{r\theta}$ at the interfaces evaluated from the measured velocity distributions in the vicinity of the interfaces. The measurement areas in the cylindrical coordinate are perfectly fitted to the spherical interface whereas the arbitrary quadrilateral measurement areas approximately represent the spherical interface as linear sides of the measurement areas. The small difference between both measured results indicates that the measurement error induced by the linear approximation of the quadrilateral measurement volume is negligible provided that the number of the measurement area is large enough.

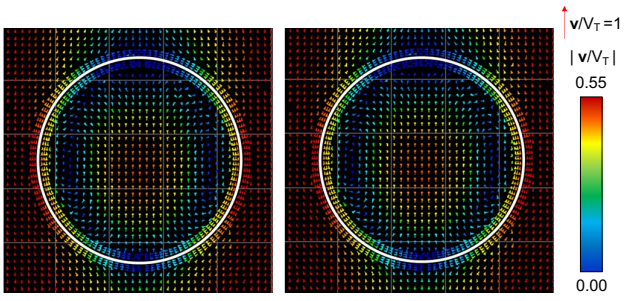

(a) Circular coordinate (b) Arbitrary quadrilateral

Figure. 4 Measured velocity distribution about single spherical drop.

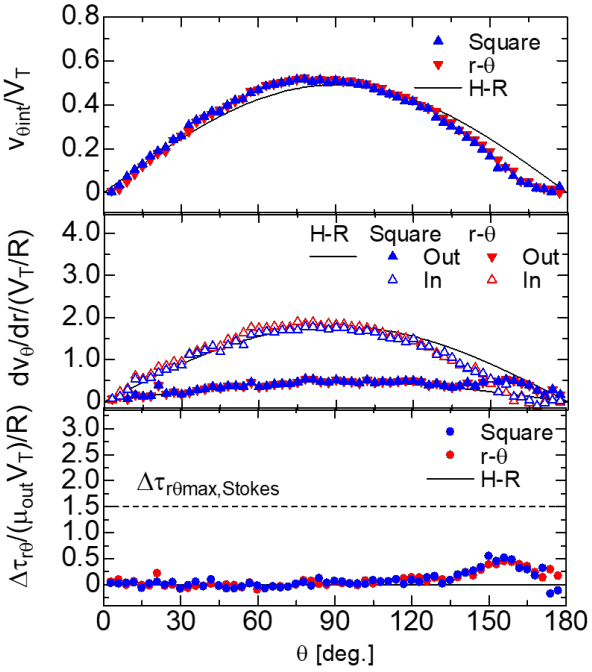

Figure. 5 Interface velocity, velocity gradient and Marangoni stress at interface.

Figure 6 shows the trajectories of tracer particles, the measured velocity distributions, and the streamlines calculated from the measured velocity distributions of single spherical, ellipsoidal, and cap drops. **Figure 7** shows $V_{\theta int}$, dV_θ/dr, and $\Delta\tau_{r\theta}$ at the interfaces evaluated from the measured velocity distributions in the vicinity of the interfaces. The streamlines agree well with the particle trajectories. No separation is observed not only in the particle trajectory but also in the measured velocity field for the spherical and ellipsoidal drops. On the other hand, the stagnant region is observed in the particle trajectory and velocity distribution in the dimple region of the tail of the cap drop. The negative velocity is observed in this region in the interfacial velocity in **Figure 7**. Hence, the separation at the tail of the cap drop can be captured by SFV. These results clearly indicate that the flow about the deformed drop is successfully measured by SFV with arbitrary quadrilateral measurement areas.

Figure 8 shows the trajectories of tracer particles, the measured velocity distributions, and the streamlines calculated from the measured velocity distributions of single ellipsoidal drops in clean and contaminated systems. **Figure 9** shows $V_{\theta int}$, dV_θ/dr, $\Delta\tau_{r\theta}$, and the surfactant concentrations Γ at the interfaces evaluated from the measured velocity distributions in the vicinity of the interfaces. Triton X-100 was used as the surfactant and its concentration in the drop ranges from 0.0 to 0.1 mol/m3. The drop tail becomes flat and then slightly dimpled shape and the internal circulation becomes weak as C increases. Even in the clean condition, Γ takes high values at the

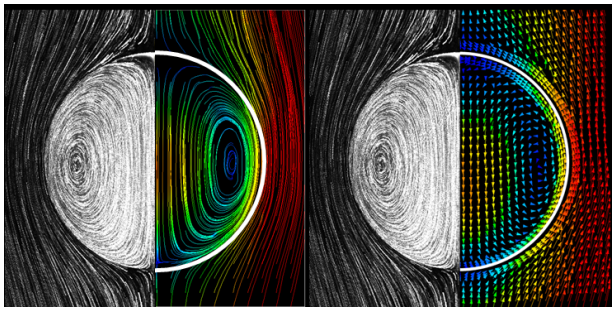

(a) Case A: Spherical drop (d = 8 mm, Re = 0.8, Eo = 3.3)

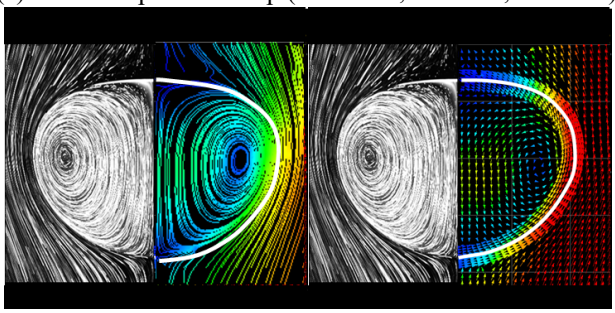

(b) Case B: Ellipsoidal drop (d = 17 mm, Re = 5.1, Eo = 13.7)

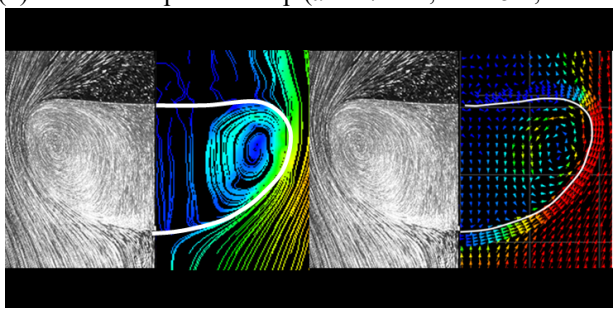

(c) Case C: Cap drop (d = 27 mm, Re = 11.7, Eo = 34.7)

Figure. 6 Measured velocity distributions about single spherical and deformed drops.

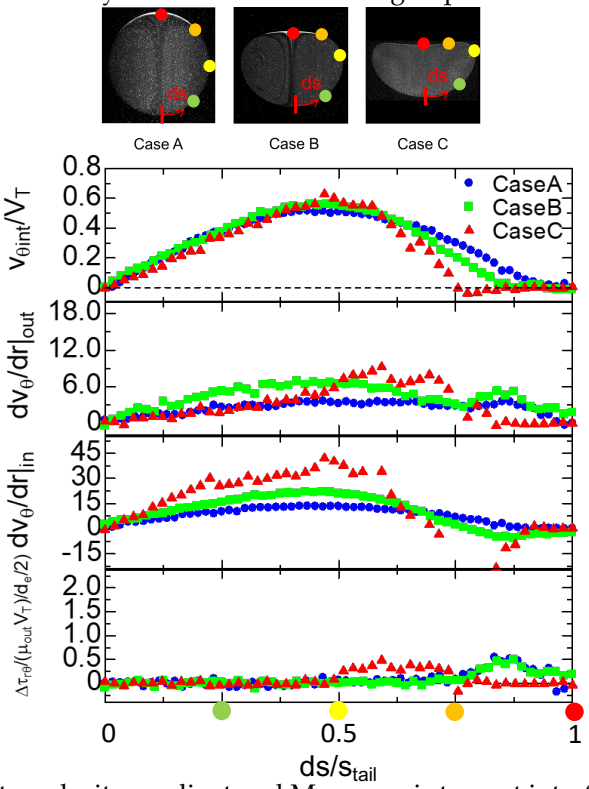

Figure. 7 Interface velocity, velocity gradient and Marangoni stress at interfaces of deformed drops.

tail region of the drop. This indicates very slight contamination is accumulated on the interface at the drop tail. As C increases, Γ reaches the maximum concentration Γ_{max} at the tail region, and Γ_{max} region extend to the front side. Hence, the maximum position of $\Delta\tau_{r\theta}$ also moves to the front direction. The Γ in the flat and slight dimple regions at the drop tail reaches to Γ_{max} and therefore the surface tension at these regions are low. The internal circulation still remain even at the high surfactant concentration condition under which the internal circulation in single spherical drop is fully damped (Hosokawa and Tomiyama, 2017).

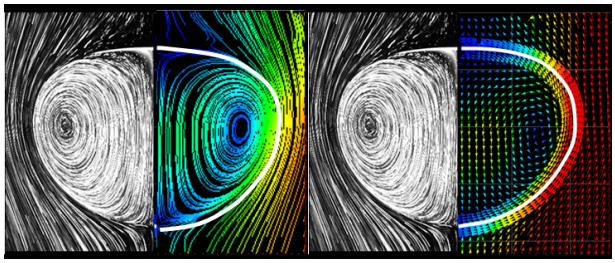

(a) Case 1: d = 17.0 mm, V_T = 0.084 m/s. C = 0.0 mol/m^3

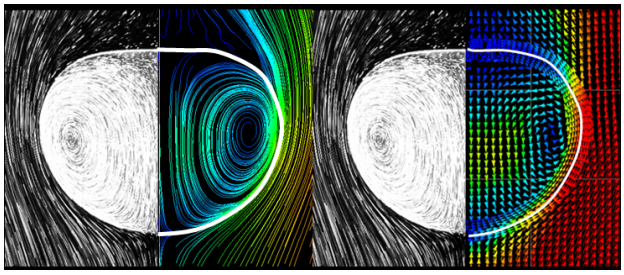

(b) Case 2: d = 17.1 mm, V_T = 0.078 m/s. C = 0.01 mol/m^3

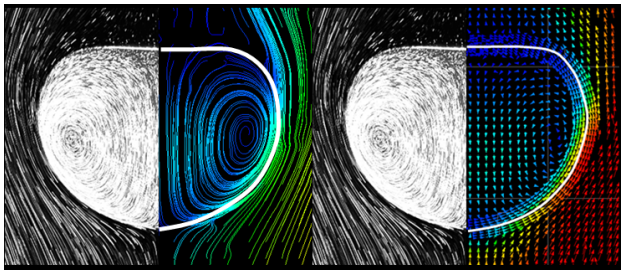

(c) Case 3: d = 16.5 mm, V_T = 0.065 m/s. C = 0.1 mol/m^3

Figure. 8 Measured velocity distributions about single deformed drops in clean and contaminated systems.

4. Conclusion

SFV is extended to arbitrary quadrilateral measurement regions fitted to an interface shape and applied to deformed single drops falling in stagnant liquid to demonstrate accurate velocity measurement in the vicinity of the deformed interface. As a result, we confirmed that the SFV successfully measured velocity distribution about single deformed drops in clean and contaminated systems, and it has the potential to evaluate viscous stress at a boundary or an interface in complex structures. The interfacial velocity, the interfacial viscous stress, the

Marangoni stress and the surface concentration of surfactant were successfully evaluated from the measured velocity distribution in the vicinity of the interface. The measured results show that the flow inside the drop and the interfacial velocity become weak as the bulk concentration of surfactant increases. However, the internal circulation remains even at the high surfactant concentration condition under which the internal circulation in a single spherical drop is fully damped.

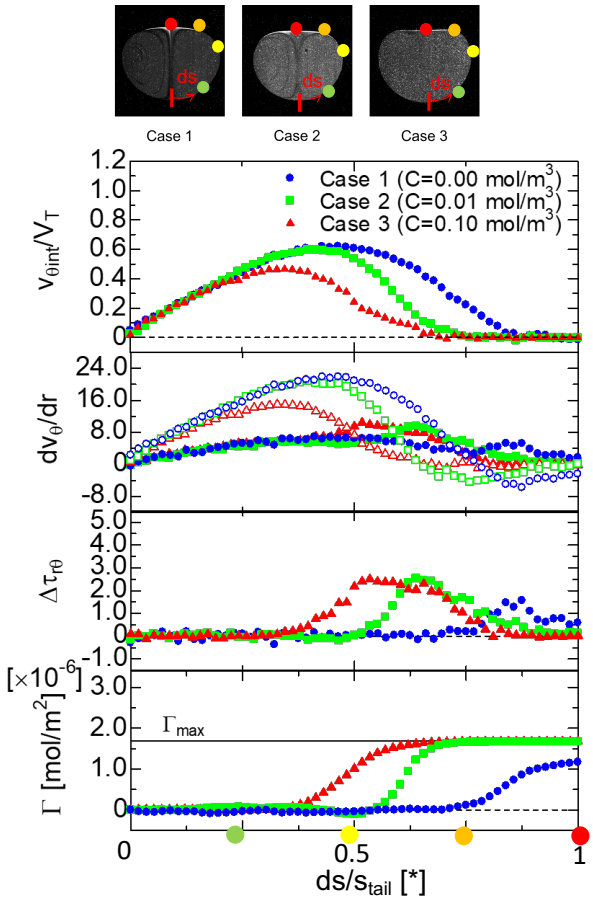

Figure. 9 Velocity, velocity gradient, Marangoni stress and surfactant concentration at contaminated drop iterfaces.

Acknowledgment

This work has been supported by Japan Society for the Promotion of Science (grand-in-aid for scientific research (B) No. 19H02067).

References

Hosokawa, S. and Tomiyama, A., Spatial Filter Velocimetry Based on Time-Series Particle Images, *Experiments in Fluids*, Vol. 52, pp. 1361–1372 (2012).

Hosokawa, S., Masukura, Y., Hayashi, K. and Tomiyama, A., Experimental Evaluation of Surfactant Concentration at an Interface of Single Spherical Drop, *International Journal of Multiphase Flow*, Vol. 97, pp. 157 – 167 (2017).

Hosokawa, S., Shigekane, G., Hayashi, K. and Tomiyama, A., Diagnostics of Flow About a Contaminated Single Drop Using Spatiotemporal Filter Velocimetry, *19th International Symposium on Applications of Laser and Imaging Techniques to Fluid Mechanics* (2018).

Ninomiya, N. and Yasuda, K., Visualization and PIV Measurement of the Flow around and inside of a Falling Droplet, *Journal of Visualization*, Vol. 9, pp. 257 – 264 (2006).